Effects of oxide-shell structures on the dynamics of oxidation of Al nanoparticles

Weiqiang Wang, Richard Clark, Aiichiro Nakano, Rajiv K. Kalia, and Priya Vashishta[a)]
Department of Chemical Engineering and Materials Science, Department of Physics and Astronomy, and Department of Computer Science, Collaboratory for Advanced Computing and Simulations, University of Southern California, Los Angeles, California 90089-0242, USA

(Received 18 January 2010; accepted 15 April 2010; published online 6 May 2010)

Effects of the crystalline and amorphous structure of alumina shells on the dynamics of oxidation of an aluminum nanoparticle (ANP) are studied using multimillion-atom molecular dynamics simulations. With an amorphous shell, formation of oxidized nanocluster fragments produced by the shattering of the shell, combined with the fragmentation and dispersion of the nanoparticle, catalyzes faster oxidation reactions. Consequently, the energy release rate of an ANP with an amorphous shell is much higher than that with a crystalline shell. Analysis on the formation of oxygen-rich fragments further confirms an enhanced reaction rate with an amorphous shell. © *2010 American Institute of Physics*. [doi:10.1063/1.3425888]

Metastable intermolecular composites (MICs) are a subclass of thermites that consist of a mixture of fuel and oxidizer particles on the nanometer scale. Nanoenergetic materials have attracted significant interest due to the higher reactivity and much faster combustion velocities than in micron-scale counterparts.[1–4] Researchers have proposed oxidation mechanisms of the aluminum nanoparticle fuel in MICs but to date no conclusive consensuses has been reached. The molecular dynamics (MD) method is a useful tool in providing atomistic details of the dynamics at the spatiotemporal scales of the reaction process of a single core-shell nanoparticle, which are seldom accessible even by the state-of-the-art experiments. In our earlier studies,[5] MD simulation was used to study the effect of the initial metallic-core temperature on the oxidation of a single aluminum nanoparticle (ANP). We found the formation of pores in the oxide shell as a principal mechanism enhancing the level of oxidative reactions in an ANP. In those studies, for simplicity, the oxide shell was taken to be crystalline. However, experimental observations by Ramaswamy *et al.*[6,7] and Gertsman and Kwok[8] have both suggested that the structure of the alumina shell of ANP is predominantly amorphous with partial crystalline regions. In experiments on the oxidation of ANP, the crystallization of the amorphous shell has also been observed.[9,10] Therefore, the effects of oxide-shell structures must be investigated in order to fully understand the oxidation of ANP.

To study the effect of the shell structure, we have performed multimillion-atom MD simulations of the oxidation process of an ANP covered with either a crystalline or an amorphous alumina shell, which will be referred as CS and AS systems, respectively. The reaction takes place in an oxygen environment, and for each system the Al core of the ANP is heated to a high temperature as in the experiments by Dlott's group.[11] The MD results demonstrate the formation of nanoclusters due to the shattering of the oxide shell as a mechanism for the extremely high reactivity of ANP when the oxide shell structure changes from crystalline to amorphous alumina.

The simulations reported here consist of a single ANP with an Al core of 40 nm diameter covered with either crystalline or amorphous alumina. The ANP is embedded in oxygen environment at 300 K. In both cases, there are 1 928 931 core Al atoms and 6 210 716 environmental O atoms. The crystalline shell consists of 1 152 528 Al and 1 727 292 O atoms. The total system consists of more than 11×10^6 atoms. The amorphous shell is prepared by first amorphizing the 4 nm thick crystalline shell and then removing the undercoordinated outermost part of the shell to give an oxide layer that is 3 nm thick. The system is then thermalized for 15 ps. The size of the MD box is taken to be sufficiently large so as to avoid boundary effects. The interatomic potentials used for Al_2O_3,[12] for metallic Al,[13] and for the oxidation process of the Al atoms are identical to that used in our previous simulations.[5] We mimic the laser flash heating experiments on ANP (Ref. 14) by heating the Al core to 9000 K while fixing the shell at room temperature. Langevin dynamics is run for an additional picosecond to heat the core uniformly. After this step, the constraints on the shell atoms are removed and the system undergoes oxidation reactions for 200 ps in a microcanonical ensemble.

To determine the effect of the shell structure on the reactivity of the ANP, we measure the energy release for both systems by plotting the increase in kinetic energy per atom averaged over all atoms as a function of time in Fig. 1(a). It

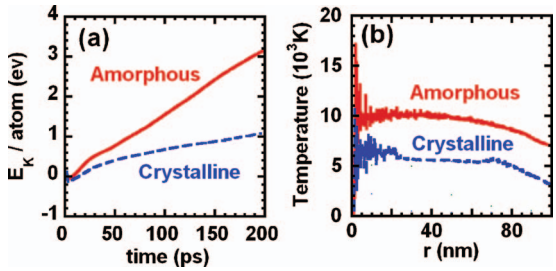

FIG. 1. (Color) (a) Increase in the kinetic energy per atom averaged over all atoms during combustion as a function of time for both crystalline and amorphous shells; (b) Temperature profile of the hot spot at 200 ps. Temperature is averaged over a 2 Å thick shell at radius of r from the center of the nanoparticle.

[a)]Electronic mail: priyav@usc.edu.

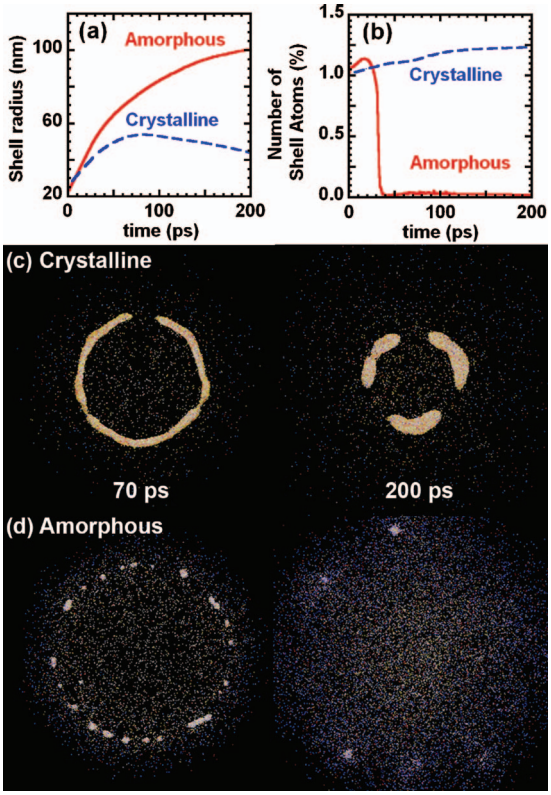

FIG. 2. (Color) Different expansion behaviors of the CS and AS systems are illustrated by (a) the radius of the ANP and (b) the percentage of atoms within the largest oxide fragment. (c) and (d) show snapshots (at 70 and 200 ps) of the center slice of CS and AS systems, respectively, with atoms color coded by species. The white color represents the Al core atoms; yellow, Al shell atoms; red, shell oxygen; and blue, the environmental oxygen. Environmental oxygen that is not covalently bonded to any Al atom is not shown for clarity of presentation.

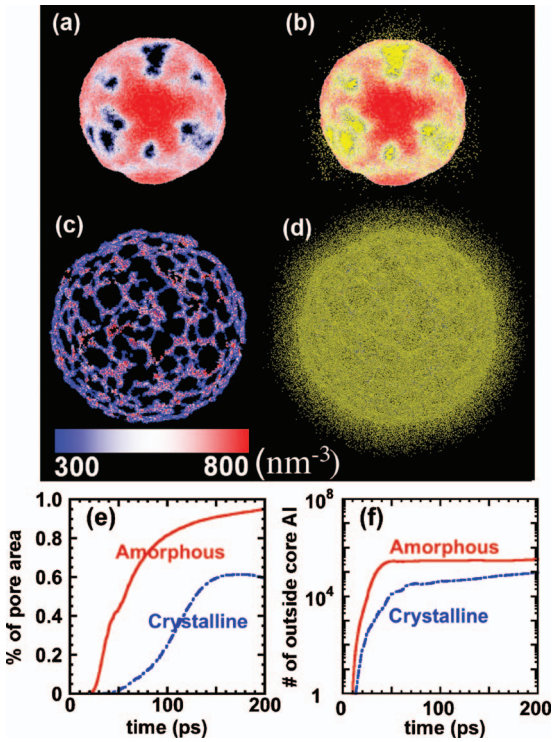

FIG. 3. (Color) (a) and (c) are snapshots of shell morphology in the CS and the AS systems, respectively, at 100 ps with colors representing the number density in the shell as shown by the color bar (in unit of number of atom per nanometer cube. (b) and (d) are snapshots of the shell morphology combined with core aluminum atoms (yellow) for the two systems. (e) Percentage of the area of pores to that of the total shell; (f) semilog plot of the number of Al core atoms jetting into the environment in both systems.

is seen that a significant amount of extra heat is produced with the amorphous shell as compared to the crystalline shell, indicating a greatly enhanced reaction rate of the ANP due to the change in the shell structure. The temperature profile of the hottest parts of the ANP at 200 ps are shown in Fig. 1(b) by plotting the temperature averaged over all atoms within a 2 Å thick spherical shell at distance r from the center of the particle (as a function of the radial distance r). It shows the formation of a larger hot spot in the amorphous-shell system as a result of greater amount of heat released. The center of the AS system is close to 10 000 K as shown in Fig. 1(b). However, the center of the CS system is around 6000 K.

In order to understand the significant difference in reaction rate and temperature profile due to the different shell structures in Fig. 1, we next examine the expansion behavior of the two systems in Fig. 2. Figure 2(a) shows the outer radius of the ANP, in which the AS system exhibits continuous expansion. In contrast, the CS system shows expansion followed by contraction. The radius is calculated as the average distance of all atoms contained within the large oxide fragments (those having over a thousand atoms) to the center of the system. Figures 2(c) and 2(d) show snapshots of the center slice of the CS and AS systems at 70 ps and 200 ps, respectively. In the three-dimensional view, the segments of the shell in the CS system in Fig. 2(c) are indeed interconnected and are part of the largest oxide fragment in the system (i.e., the shell with pores).

However, in the AS system, the fragments shown in Fig. 2(d) are disconnected, indicating shattered pieces of the shell. This shattering of the amorphous shell can also be seen quantitatively by comparing the percentage of atoms in the largest oxide fragment at a given time to that at the beginning of the simulation, see Fig. 2(b). At 0 ps, the largest oxide fragment is the shell in both systems. Figure 2(b) shows that the number of the atoms in the shell in the CS system increases continuously due to oxidation reactions on the shell surface but it decreases by several orders of magnitude in the AS system, indicating that the shattering of the shell. Continuous oxidation of the shell in the CS system [Fig. 2(c)] protects the Al core it encloses from oxidation, resulting in the slower reaction rate in the CS system. On the other hand, all the fragments in the AS system are small [Fig. 2(d)]. Aluminum atoms in these fragments are mostly undercoordinated and prone to further oxidation. This partially accounts for the faster energy release rate of the AS system seen in Fig. 1(a).

The other factor responsible for the faster energy release rate in the AS system is the increased amount of core Al atoms that jet out into the surrounding oxygen and are able to be directly oxidized by the environmental oxygen, as seen in Fig. 3. Figures 3(a) and 3(c) show the projected view of the CS and AS shells, respectively, at 100 ps with colors indicating the local number density within the shell. Figures 3(b) and 3(d) show the core Al (colored yellow) jetting out of the CS and AS shells, respectively. In both systems, there are many core Al jetting out, causing direct, and thus faster, oxidation reactions. But spatial symmetries of the crystalline structure result in symmetric pores in the CS shell [see Fig.

TABLE I. Number of fragments of various chemical compositions in CS and AS systems at 200 ps.

	Al_4O	Al_3O	Al_2O	AlO	Al_2O_3	AlO_2
Crystalline shell	126	655	6107	98 828	3185	113 796
Amorphous shell	7	96	16 643	686 650	58 798	742 613

3(a)]. In contrast, the formation of pores occurs randomly in the AS shell [Fig. 3(c)]. Opening of pores in the crystalline shell results in less overall area for the core Al to move through. This is seen quantitatively from Figs. 3(e) and 3(f). Figure 3(e) plots the area percentage of the pores of the shell, whereas Fig. 3(f) plots the number of core Al that jet out. We see that the amorphous shell has a much larger area corresponding to pores. As a result, far more core Al jet out in the AS system, resulting in more direct oxidations in the surrounding oxygen and a faster heat release. This is consistent with the energy release rate curves in Fig. 1.

To compare the reaction rates of these two systems, we have also investigated the intermediate oxide products using fragment analysis. Both simulations[15,16] and experiments[14,17,18] have observed intermediate aluminum oxide products with a variety of aluminum-oxygen ratios. In particular, it is found that AlO and AlO_2 are the two primary intermediates that give rise to the final product Al_2O_3. In our simulations, oxide fragments are identified by the atoms that are covalently bonded. At 200 ps, the majority of fragments in both systems are found to be small, having less than six atoms. The only fragment having more than 500 atoms in the CS system is the shell, consisting of 3 544 013 atoms. In the AS system, there are only 83 fragments having more than 1000 atoms, the largest having 22 631 atoms. Statistics of number of various fragments are listed in Table I, which shows that the AS system has much more number of oxygen rich fragments as compared to that of the CS system. Figure 4 shows the production of AlO, AlO_2, and Al_2O fragments in the two systems in the reaction process, with (a) showing the number of each type of fragment and (b) what percentage of all fragments is made of each type. We found that, in both systems, the number of Al_2O fragments decreases after an initial increase, and the AlO and AlO_2 fragments become more numerous. However, the number of fragments of each type in the AS system far exceeds those in the CS system [Fig. 4(a)]. Figure 4(b) shows that the majority of the fragments in both systems change from Al-rich to oxygen-rich in less than 50 ps. Although both systems follow this trend, the transition occurs much faster in the AS system, indicating a faster reaction rate.

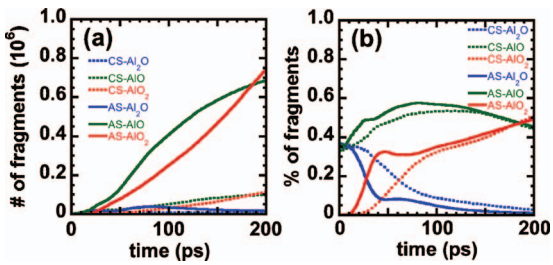

FIG. 4. (Color) Production of Al_2O (blue), AlO (green), and AlO_2 (red) fragments in the CS (dashed lines) and AS (solid lines) systems are shown by (a) number of fragments of each species and (b) the relative percentage of each fragment species.

In summary, we have found that an ANP covered with amorphous oxide-shell has much higher reactivity than that with crystalline shell. The crystalline shell expands and then shrinks, resulting in pore opening and the ejection of core Al atoms into the surrounding oxygen where fast oxidation occurs. However, in the crystalline system, there is a considerable amount of core aluminum that remains covered by the shell. In contrast, an ANP with amorphous shell continuously expands and shatters, resulting in only small oxide fragments and Al clusters which are prone to rapid oxidation. The shattering of the amorphous shell also results in a larger area of the shell opening into pores, resulting in a much faster and widespread oxidation of the core Al atoms that jet out.

This work was supported by the Basic Research Program of Defense Threat Reduction Agency Grant Nos. HDTRA10710023 and HDTRA10810036. Simulations were performed at the CACS and HPC center at USC. We thank Dr. Suhithi Peiris for stimulating discussions.

[1] S. F. Son, B. W. Asay, T. J. Foley, R. A. Yetter, M. H. Wu, and G. A. Risha, J. Propul. Power **23**, 715 (2007).
[2] K. K. Kuo, G. A. Risha, B. J. Evans, and J. E. Boyer, Mater. Res. Soc. Symp. Proceedings No. 800 (Materials Research Society, Pittsburgh, 2004), p. A1.1.1–12.
[3] V. I. Levitas, B. W. Asay, S. F. Son, and M. Pantoya, J. Appl. Phys. **101**, 083524 (2007).
[4] K. Zhang, C. Rossi, G. A. A. Rodriguez, C. Tenailleau, and P. Alphonse, Appl. Phys. Lett. **91**, 113117 (2007).
[5] W. Wang, R. Clark, A. Nakano, R. K. Kalia, and P. Vashishta, Appl. Phys. Lett. **95**, 261901 (2009).
[6] A. L. Ramaswamy and P. Kaste, J. Energ. Mater. **23**, 1 (2005).
[7] A. L. Ramaswamy, P. Kaste, and S. F. Trevino, J. Energ. Mater. **22**, 1 (2004).
[8] V. Y. Gertsman and Q. S. M. Kwok, Microsc. Microanal. **11**, 410 (2005).
[9] Q. S. Mei, S. C. Wang, H. T. Cong, Z. H. Jin, and K. Lu, Acta Mater. **53**, 1059 (2005).
[10] A. Rai, D. Lee, K. Park, and M. R. Zachariah, J. Phys. Chem. B **108**, 14793 (2004).
[11] Y. Q. Yang, S. F. Wang, Z. Y. Sun, and D. D. Dlott, J. Appl. Phys. **95**, 3667 (2004).
[12] P. Vashishta, R. K. Kalia, A. Nakano, W. Li, and I. Ebbsjo, *Amorphous Insulators and Semiconductors* (Kluwer, Dordrooht, 1996), p. 151.
[13] A. F. Voter, in *Intermetallic Compounds*, edited by J. H. Westbrook and R. L. Fleischer (Wiley, New York, 1994), Vol. 1, p. 77.
[14] S. F. Wang, Y. Q. Yang, Z. Y. Sun, and D. D. Dlott, Chem. Phys. Lett. **368**, 189 (2003).
[15] T. J. Campbell, G. Aral, S. Ogata, R. K. Kalia, A. Nakano, and P. Vashishta, Phys. Rev. B **71**, 205413 (2005).
[16] A. Hasnaoui, O. Politano, J. M. Salazar, G. Aral, R. K. Kalia, A. Nakano, and P. Vashishta, Surf. Sci. **579**, 47 (2005).
[17] G. I. Pangilinan and T. P. Russel, J. Chem. Phys. **111**, 445 (1999).
[18] T. N. Piehler, F. C. Delucia, C. A. Munson, B. E. Homan, A. W. Miziolek, and K. L. Mcnesby, Appl. Opt. **44**, 3654 (2005).